The Astrophysical Journal, 961:182 (11pp), 2024 February 1 https://doi.org/10.3847/1538-4357/ad118e

What is the Reynolds Number of the Solar Wind?

Daniel Wrench[1], Tulasi N. Parashar[1], Sean Oughton[2], Kevin de Lange[1], and Marcus Frean[1]
[1] Victoria University of Wellington, Kelburn, Wellington 6012, New Zealand; daniel.wrench@vuw.ac.nz
[2] University of Waikato, Hamilton 3240, New Zealand
Received 2023 October 9; revised 2023 November 21; accepted 2023 November 22; published 2024 January 25

Abstract

The Reynolds number, *Re*, is an important quantity for describing a turbulent flow. It tells us about the bandwidth over which energy can cascade from large scales to smaller ones, prior to the onset of dissipation. However, calculating it for nearly collisionless plasmas like the solar wind is challenging. Previous studies have used formulations of an "effective" Reynolds number, expressing *Re* as a function of the correlation scale and either the Taylor scale or a proxy for the dissipation scale. We find that the Taylor scale definition of the Reynolds number has a sizable prefactor of approximately 27, which has not been employed in previous works. Drawing from 18 years of data from the Wind spacecraft at 1 au, we calculate the magnetic Taylor scale directly and use both the ion inertial length and the magnetic spectrum break scale as approximations for the dissipation scale, yielding three distinct *Re* estimates for each 12 hr interval. Average values of *Re* range between 116,000 and 3,406,000 within the general distribution of past work. We also find considerable disagreement between the methods, with linear associations of between 0.38 and 0.72. Although the Taylor scale method is arguably more physically motivated, due to its dependence on the energy cascade rate, more theoretical work is needed in order to identify the most appropriate way of calculating effective Reynolds numbers for kinetic plasmas. As a summary of our observational analysis, we make available a data product of 28 years of 1 au solar wind and magnetospheric plasma measurements from Wind.

Unified Astronomy Thesaurus concepts: Solar wind (1534); Interplanetary turbulence (830); Magnetohydrodynamics (1964); Space plasmas (1544)

1. Introduction

Most naturally occurring plasmas are either observed to be or believed to be in a turbulent state. There is significant variation in the parameters of these systems, including the length and timescales, the plasma β, the turbulent Mach numbers, and the relative size of the system compared to kinetic scales. Many of these systems are in what is called a "kinetic" state, where the dynamical length and timescales of interest are comparable to or smaller than the collisional timescales of interest. Astrophysical examples include the solar wind (e.g., Bruno & Carbone 2013), accretion disks (e.g., Balbus & Hawley 1998), and the intracluster medium (e.g., Mohapatra et al. 2020). For these systems, the collisional closures associated with fluid models are no longer applicable (or at least not obviously so). This means one has to resort to higher-order closures for the fluid models, or, in most cases, to a kinetic description of the plasma (e.g., Marsch 2006).

Turbulence theories utilize dimensionless parameters to categorize various flow regimes. For homogeneous incompressible Navier–Stokes turbulence, the most important of these is the Reynolds number *Re*, defined as the ratio of the characteristic magnitudes of the nonlinear inertial term and the viscous term of the Navier–Stokes momentum equation (e.g., Pope 2000). Herein we define it by

$$Re = \frac{U\lambda_C}{\nu}, \tag{1}$$

where $U = \sqrt{\langle \boldsymbol{v} \cdot \boldsymbol{v} \rangle}$ is the characteristic rms speed of the fluctuations, λ_C is the correlation scale (or outer scale), and ν is the (kinematic) viscosity; $\boldsymbol{v}(\boldsymbol{x}, t)$ is the velocity field. Loosely, λ_C corresponds to the largest separation at which turbulent fluctuations remain correlated, which in a hydrodynamic context can be thought of as the size of the energy-containing eddies. (It is also often written as L and called the "characteristic length" scale.) Small *Re* implies that the viscous effects are significant and hence the nonlinear term is weak and will not introduce significant nonlinearities into the system's evolution. Conversely, a large value of *Re* implies that the nonlinear term plays a significant role in the dynamics of the fluid.

This dynamic can be appreciated more clearly when *Re* is expressed solely in terms of length scales. One way this can be done is to introduce the Kolmogorov dissipation scale (or inner scale) $\eta = (\nu^3/\epsilon)^{1/4}$, where $\epsilon = \nu\langle(\nabla \times \boldsymbol{v})^2\rangle$ is the mean rate of kinetic energy dissipation (Kolmogorov 1941; Tennekes & Lumley 1972). A physical interpretation is that the Kolmogorov scale is where the smallest eddies in the fluid become critically damped, due to their nonlinear (or turnover) timescale being equal to their dissipation timescale. Recall also that the dissipation rate can be phenomenologically modeled as

$$\epsilon_{\text{phenom}} = C_\epsilon \frac{U^3}{\lambda_C}, \tag{2}$$

where C_ϵ is treated as a fitting constant (e.g., Batchelor 1970; Tennekes & Lumley 1972). Employing this in the definition of η yields the form

$$Re \equiv Re_\eta = \frac{1}{C_\epsilon^{1/3}} \left(\frac{\lambda_C}{\eta}\right)^{4/3}, \tag{3}$$

revealing that *Re* is a measure of the bandwidth of the turbulent energy cascade. A large *Re* indicates there is a large separation

between the outer and inner scales. This larger bandwidth implies there are more scales where the nonlinear term is strong enough to create turbulent structures and thereby increase the intermittency of the flow (see, e.g., Matthaeus et al. 2015; Parashar et al. 2019; Cuesta et al. 2022b). A small bandwidth, and hence a small *Re*, implies that dissipation occurs very quickly and damps any turbulent structures that the nonlinear term might try to create. Such low-*Re* situations are sometimes seen in planetary magnetosheaths (Czaykowska et al. 2001; Hadid et al. 2015; Huang et al. 2017; Chhiber et al. 2018).

Estimating *Re* for hydrodynamical systems, using Equation (1), is straightforward as all the required quantities are well defined and often readily determined in experiments. For kinetic plasmas such as the solar wind, however, it is not possible to write a Chapman–Enskog-like closure to define a viscosity (Chapman & Cowling 1990; Huang 2008). (Some attempts have been made to estimate the viscosity of kinetic systems; see, e.g., Verma 1996; Zhuravleva et al. 2019; Bandyopadhyay et al. 2023; Yang et al. 2023.) This lack of a well-defined viscosity also precludes using Equation (3), as it means we cannot define η. Typically, in kinetic plasmas, one must therefore resort to defining an *effective* Reynolds number. Some hydrodynamic studies have investigated estimating the energy input into the system (Zhou et al. 2014), as well as using more precise boundaries of the inertial range (Zhou 2007; Zhou & Thornber 2016), in order to get around this lack of a clearly defined inner scale. Herein we describe two approaches to formulating an effective Reynolds number.

The first approach is to apply Equation (3) and use a different small scale—one that is observationally calculable—as a signifier of the termination of the inertial range. There are several reasonable options to choose from. For example, in the solar wind, the *spectral break scale*, f_b, the point at which the power spectrum of the inertial range steepens, is thought to be a good indicator of the onset of dissipation (Leamon et al. 1998; Yang et al. 2022). Additionally, the *ion inertial length*, d_i, and also the ion gyroradius are frequently found to be in proximity to the break scale, motivating their use as indicators of the onset of the kinetic range (Chen et al. 2014; Franci et al. 2016; Wang et al. 2018; Woodham et al. 2018; Parashar et al. 2019; Cuesta et al. 2022b; Lotz et al. 2023). We note that d_i has the advantage that it only requires ion density to calculate, rather than the high-resolution magnetic field data needed to resolve spectral-steepening scales and calculate f_b. Its disadvantage is that it does not capture the size of the turbulence amplitudes. For example, consider the two different intervals in Figure 1, each with very similar d_i and outer scales λ_C but with different turbulence amplitudes. The use of d_i as an inner scale in Equation (3) consequently yields very similar Re_{d_i} for both cases because it does not capture the different dynamics induced by the varying turbulence strengths.

Fortunately, there is a length scale that typically does depend on the energy of the turbulent fluctuations due to their effect on the shape of the power spectrum. This is the Taylor microscale λ_T (Taylor 1935; Batchelor 1970; Matthaeus et al. 2008), hereafter referred to simply as the Taylor scale. See Figure 1 for one such example. By employing it in a further reformulation of *Re* we can capture this strength-of-the-turbulence aspect. The Taylor scale has multiple definitions and can be estimated in several different ways that differ by factors of order unity (denoted below by γ). These can all be written, for the velocity field $\boldsymbol{v}$, as

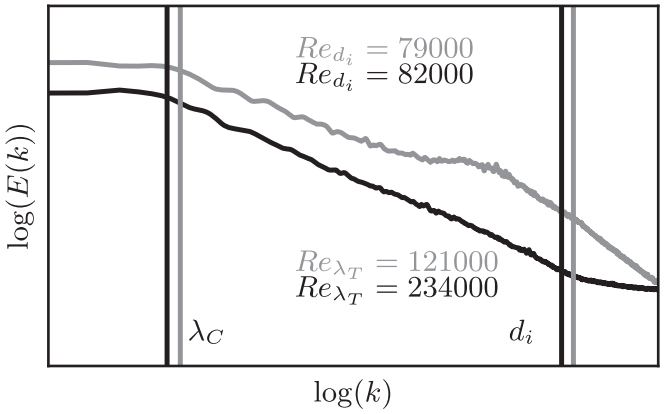

Figure 1. Power spectra (energy $E(k)$ vs. wavenumber k) for two spacecraft data intervals with very similar outer and inner scales but different power levels. Vertical lines indicate the respective correlation scales λ_C and ion inertial lengths d_i. On the basis of the power levels one would expect different turbulent behavior from these intervals. However, using d_i as the inner scale in Equation (3) implies they have almost the same *Re*. Using Equation (5) we do capture this difference, giving very different values of Re_{λ_T}.

$$\lambda_T^2 = \gamma \frac{\langle \boldsymbol{v}^2 \rangle}{\langle (\nabla \times \boldsymbol{v})^2 \rangle}, \tag{4}$$

where the value of γ depends on the specific definition of λ_T employed. For example, the traditional hydrodynamics usage is that λ_T is the curvature (at the origin) of the longitudinal autocorrelation function so that $\gamma = 5$ (e.g., Batchelor 1970; Tennekes & Lumley 1972, p. 211). Herein we employ $\gamma = 3$ because it corresponds to the curvature of the *traced* correlation function, which is relatively simple to calculate using spacecraft time series data; see Equations (7) and (8).

The inertial range comprises the scales ℓ, which satisfy $\eta \ll \ell \ll \lambda_C$. Moreover, in hydrodynamics λ_T lies between λ_C and the Kolmogorov scale (e.g., Pope 2000). Equation (4) makes it clear that λ_T is related to the mean square spatial derivatives of the turbulent flow. It can also be interpreted as the "single-wavenumber equivalent dissipation scale" (Hinze 1975). In plasma systems, the Taylor scale represents small-scale turbulence physics that is not yet well understood, including its relationship to other plasma parameters and the correlation length.

Re-expressed in terms of the Taylor scale, the exact hydrodynamic viscous dissipation rate is $\epsilon = \nu\gamma \langle \boldsymbol{v}^2 \rangle / \lambda_T^2$. Equating this to the $\epsilon_{\rm phenom}$ relation, Equation (2), yields another form for the Reynolds number (Batchelor 1970, p. 118; Tennekes & Lumley 1970, p. 67):

$$Re \equiv Re_{\lambda_T} = \frac{\gamma}{C_\epsilon} \left(\frac{\lambda_C}{\lambda_T} \right)^2. \tag{5}$$

The ratio of Taylor scale to the spectral break scale has been shown to have a direct correlation with the decay rate (Matthaeus et al. 2008). Hence, one would expect this definition of *Re* to show variation with changing turbulence amplitude and decay rates (as can be seen from the very different values of Re_{λ_T} in Figure 1).

Note that C_ϵ is significantly less than unity. Hydrodynamic simulations and experiments (Sreenivasan 1998; Pearson et al. 2004)

indicate that

$$C_\epsilon \approx 0.5\frac{2}{9\sqrt{3}} \approx \frac{1}{15.6}, \quad (6)$$

where in the middle term the 0.5 value is empirical and the other values are associated with "unit conversion" from a variant of Equation (2) commonly used in the hydrodynamic literature, namely $\epsilon_{\rm phenom} = Au_{\rm l}^3/\ell_f$; here $U^2 = 3u_{\rm l}^2$ and $\ell_f = 3\lambda_C/2$ is the correlation length for the longitudinal velocity correlation function, all assuming isotropy (see, e.g., Batchelor 1970; Tennekes & Lumley 1972; Pearson et al. 2004). Thus, in hydrodynamics, with $\gamma = 3$, the prefactor in Equation (5) is $\gamma/C_\epsilon \approx 50$, and in Equation (3) it is $C_\epsilon^{-1/3} \approx 3$. The values in MHD, for solar wind-like conditions, are $\gamma/C_\epsilon \approx 27$ and $C_\epsilon^{-1/3} \approx 2$ (see Appendix A). These are the values we use in the data analysis reported on below. However, one should keep in mind that these values pertain to collisional MHD fluid models. The solar wind is an almost collisionless plasma that can, in some circumstances, be well approximated as an MHD fluid.

For a system like the solar wind, most velocity measurements have a time cadence that is significantly longer than kinetic timescales (with the exception of measurements from the Magnetospheric Multiscale (MMS) mission). Because of this, one cannot reliably compute $\lambda_{\rm T}$ for the velocity field. On the other hand, magnetic field measurements have a significantly higher time cadence, allowing one to explore kinetic-scale physics. Hence most studies in the solar wind compute the Taylor scale for the magnetic field. Given these constraints, we also work (primarily) with magnetic field data in this study and compute several types of *effective* Reynolds numbers.

A history of estimating magnetic *Re* in the solar wind is provided in the introduction to Cartagena-Sanchez et al. (2022). Prior estimations have used Equation (5) and applied it to measurements from multiple spacecraft, beginning with Matthaeus et al. (2005) and continuing with Weygand et al. (2007, 2009, 2011) and Zhou et al. (2020). Note that these studies use $\gamma/C_\epsilon = 1$, and thus essentially ignore this prefactor. The average values of λ_C, $\lambda_{\rm T}$, and $Re_{\lambda_{\rm T}}$ from these studies are summarized in Table 2, where we also indicate an appropriate value of γ/C_ϵ to be used for comparison with the results we obtain herein. All these studies used data from a combination of spacecraft at 1 au, including ACE, Wind, and Cluster, and most investigated the relationship between *Re* and variables such as magnetic field orientation, wind speed, and solar activity. Going beyond 1 au, this formulation has also been used to estimate *Re* at Mars (Cheng & Wang 2022), and Voyager data have been used to calculate it at very large distances from the Sun (Parashar et al. 2019). Voyager data lack sufficient resolution to calculate $\lambda_{\rm T}$, and thus d_i was used in the formulation of Equation (3) to estimate *Re*. Cuesta et al. (2022b) supplemented this work with data from Parker Solar Probe and Helios in a survey of variation in *Re* throughout the heliosphere.

It is clear from the studies cited above that the Reynolds number plays a pivotal role in understanding solar wind turbulence. Accurate estimation of *Re* can be used to validate theoretical predictions such as the enhanced intermittency with increasing *Re* (e.g., Van Atta & Antonia 1980; Parashar et al. 2015, 2019; Cuesta et al. 2022b) or its correlation with solar activity (Zhou et al. 2020; Cheng & Wang 2022). Different formulations need to be compared to bolster these conclusions further. Additionally, a firmer estimate of *Re* will help refine the minimum scale separation required by an experiment or simulation to faithfully capture the dynamics of such high-*Re* astrophysical systems; this is the so-called "minimum state" (Zhou 2007, 2017). Therefore, to obtain reliable estimates of the solar wind's (effective) Reynolds number, a thorough comparison of computational techniques and their implications is necessary.

This is the purpose of the present study. A large data set of measurements from the Wind spacecraft is compiled, allowing us to calculate *Re* for nearly two decades of data in three different ways: using either f_b (obtained from the magnetic energy spectrum) or d_i in Equation (3), and using $\lambda_{\rm T}$, obtained from the autocorrelation function for $\boldsymbol{b}$, in Equation (5).

The structure of this paper is as follows. The data set and its initial cleaning are described in Section 2. Section 3 provides the methods for estimating each of the scales; we calculate $Re_{\lambda_{\rm T}}$ after first applying the correction to $\lambda_{\rm T}$ developed by Chuychai et al. (2014). In Section 4, the three estimators are compared to each other and to the values obtained by the aforementioned studies. Implications and limitations of these results are discussed in Section 5.

2. Data

We use roughly 18 years (2004–2022) of data from NASA's Wind spacecraft to estimate *Re* at 1 au. We process ≈12,000 12 hr intervals in the solar wind. High-resolution (0.092 s) vector magnetic field data were obtained from the Magnetic Field Investigation (MFI; Lepping et al. 1995). Wind was launched in 1994 and has operated at the Lagrangian point 1 (L1) since 2004 June in order to study plasma processes occurring in the near-Earth solar wind. This mission has significantly contributed to understanding many aspects of the solar wind, including electromagnetic turbulence (Wilson et al. 2021).

After downloading the data from NASA/GSFC's Space Physics Data Facility (SPDF), we split them into 12 hr intervals. This interval size is large enough to contain a few correlation lengths but small enough to not average over large-scale variations. Isaacs et al. (2015) demonstrated that (1 au) intervals of 10–20 hr have "special significance" as they represent a range where sufficient correlation times are sampled, making single-spacecraft results coincide with those of multiple spacecraft.

Data gaps are linearly interpolated unless they comprise more than 10% of the interval, in which case the interval is discarded. (This affected about 4% of the intervals.) We initially processed 28 years of data, from 1995 January 1 to 2022 December 31, to compute various average quantities as well as turbulence parameters such as the spectral slopes in the inertial and kinetic ranges, rms amplitudes of the magnetic field and velocity, the Taylor scale, and the correlation scale. The complete data set comprises all available magnetic field data, i.e., intervals containing shocks or from within the Earth's magnetosphere are *not* removed. However, our analysis in the subsequent sections of this paper focuses only on data from 2004 June and later, a period when Wind was positioned at L1, away from the magnetosphere.

Given that it is also of interest to future analysis how quantities like the Taylor scale relate to other properties of the

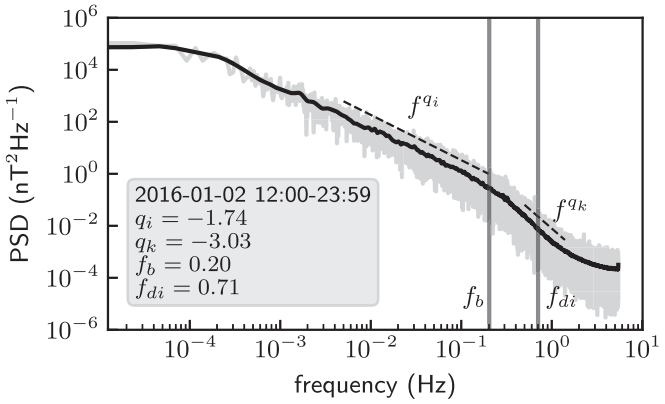

Figure 2. Power spectral density (PSD) of a solar wind magnetic field interval, raw (gray) and smoothed (black). Dashed power-law fits to estimates of the inertial and kinetic ranges return spectral indices q_i and q_k. The left-hand vertical line indicates the intersection of these two fits, denoted as the spectral break f_b; the ion inertial frequency f_{d_i} is indicated by the right-hand vertical line.

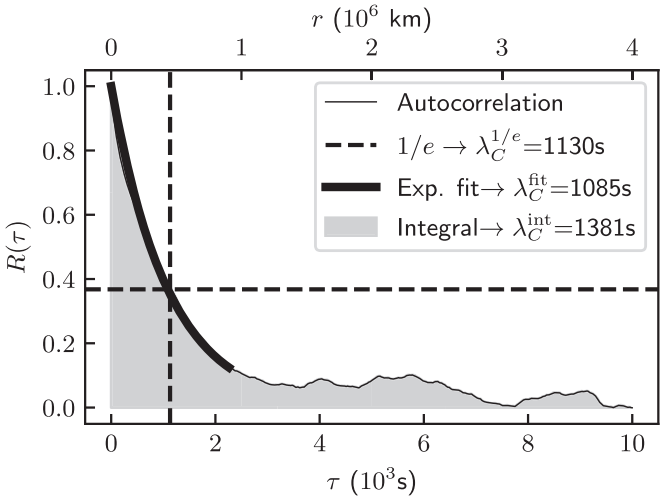

Figure 3. A demonstration of the three methods used to calculate λ_C using an interval comprising the second half of 2016 January 2. These include the $1/e$ ("e-folding") method, giving $\lambda_C^{1/e}$; the exponential fit method, giving $\lambda_C^{\rm fit}$; and the integral method, giving $\lambda_C^{\rm int}$.

turbulent plasma system—such as electron density, cross-helicity, and solar activity—measurements of electron and proton properties from Wind's 3D Plasma (3DP) instrument were also obtained, along with sunspot numbers from the World Data Center SILSO.

We note that the ion density from Wind has periods of anomalously small values for a few months. To avoid issues associated with this we therefore always use the electron density as a proxy for the proton density when calculating all ion inertial lengths, ion plasma betas, and Alfvén speeds. Across the 28 years of data, we obtained between 18,000 and 20,000 points for each variable, depending on the amount of missing data. A full list of the variables in the processed (and publicly available) data set can be found in Appendix B.

3. Method

We begin the analysis by determining several slopes for each of the magnetic power frequency spectra obtained from the 12 hr intervals. Specifically, we perform power-law fits in the inertial and kinetic ranges, denoting the power-law exponents as q_i and q_k, respectively. Nominal frequency intervals for the inertial range (0.005–0.2 Hz) and kinetic range (0.5–1.4 Hz) were chosen, consistent with those used by Wang et al. (2018). We then identify the frequency at which (the extrapolations of) these power laws intersect, calling this the spectral break frequency f_b. An example is shown in Figure 2. Any outliers, mostly in the form of anomalously large values of q_k, are not included in the subsequent analysis, as described in Section 4. In the following, we will use the timescale associated with the break frequency, i.e., $t_b = 1/(2\pi f_b)$, as a proxy for the inner (time)scale.

Estimates for the Taylor scale $\lambda_{\rm T}$ and the correlation scale λ_C are also needed and these are both computed using the autocorrelation functions (see Figure 26 in Bruno & Carbone 2013). The (normalized) temporal autocorrelation of the magnetic field fluctuations is given by

$$R(\tau) = \frac{\langle \boldsymbol{b}(t) \cdot \boldsymbol{b}(t+\tau) \rangle}{\langle \boldsymbol{b}^2 \rangle}, \tag{7}$$

where $\boldsymbol{b}(t) = \boldsymbol{B}(t) - \langle \boldsymbol{B}(t) \rangle$ is the magnetic field fluctuation at time t. The angle brackets denote a suitable time ensemble average, implemented as a time average in this study. Using Taylor's frozen-in-flow hypothesis, we can convert time separations τ into length separations r. (See Section 5 for a discussion of the limitations of this hypothesis.)

Measurement of λ_C requires a computation of the autocorrelation function out to very large lags. On the other hand, measurement of $\lambda_{\rm T}$ requires iterative fitting at very small lags. It would quickly become computationally expensive to use the high-time-cadence data to obtain both quantities. Hence, for each 12 hr interval, the correlation length λ_C is computed from a downsampled low-resolution (5 s) magnetic field time series out to roughly 10,000 s. We use the high-time-cadence (0.092 s) magnetic field data to compute autocorrelation functions only up to a lag of 9.2 s; this is used to compute the magnetic Taylor scale $\lambda_{\rm T}$.

The correlation scale λ_C for $\boldsymbol{b}$ can be estimated from $R(\tau)$ in three different ways, as shown in Figure 3. We can perform an exponential fit, we can find the separation at which the function falls to $1/e$, or we can take the integral of the function ($\lambda_C = \int_0^\infty R(\tau)\, d\tau$). The exponential fit method is frequently used in the literature (Matthaeus et al. 2005; Bandyopadhyay et al. 2020; Zhou et al. 2020; Phillips et al. 2022); multiple exponential fits and a third-order polynomial have also been used (Weygand et al. 2009, 2011; Cheng & Wang 2022). In any case, this requires a decision about how much of the autocorrelation to fit to. In this work, we fit a single exponential to a range that extends to twice the value of the correlation scale as obtained by the $1/e$ method. We compute λ_C from the low-resolution autocorrelation using each of these three methods to evaluate their consistency.

While it is straightforward to compute the Taylor scale in simulations, where one has access to the full three-dimensional information, when working with time series data from experiments we need to resort to an approximation. Since $\lambda_{\rm T}$ can be defined as the radius of curvature of the autocorrelation function at the origin, we may use this definition to estimate it. (We do not yet need to convert to spatial lags, so we work with the time-domain equivalent, $\tau_{\rm TS}$.) This follows from the Taylor expansion of the autocorrelation for $\tau \rightarrow 0$ (Batchelor 1970;

Tennekes & Lumley 1972):

$$R(\tau) = 1 - \frac{\tau^2}{2\tau_{\rm TS}^2} + \ldots . \quad (8)$$

In practice, this means fitting a parabola to $R(\tau)$ at the origin and requires the high-resolution data provided by Wind so that we have enough observations at small separations. It also requires an important decision: how much of this high-resolution autocorrelation do we fit to? (Larger ranges result in systematically larger estimates.) In order to reduce the subjectivity of this decision, the Richardson extrapolation technique was introduced in this context by Weygand et al. (2007): by fitting to a range of values of maximum lag $\tau_{\rm fit}$, then extrapolating back to 0 lags, we obtain a refined estimate, $\tau_{\rm TS}^{\rm ext}$. In the aforementioned work, the authors showed an apparent convergence of the final estimate given by this technique as $\tau_{\rm fit}$ increases. However, Chuychai et al. (2014) showed with simulated data that, in fact, this convergence depends upon the slope of the power spectrum at high frequencies. In light of this, they produced a multiplicative correction factor, $r(|q|)$, that is a function of this slope, given as

$$r(|q|) = \begin{cases} -0.64\left(\frac{1}{|q_k|}\right) + 0.72, & \text{when } |q_k| < 2 \\ -2.61\left(\frac{1}{|q_k|}\right) + 1.70, & \text{when } 2 \leqslant |q_k| < 4.5 \\ -0.16\left(\frac{1}{|q_k|}\right) + 1.16, & \text{when } |q_k| \geqslant 4.5. \end{cases} \quad (9)$$

We also apply this correction to our estimates, with the procedure we follow depicted in Figure 4. This gives us a final estimate $\tau_{\rm TS}$. We fit from a minimum lag of 1, equal to the time cadence (0.092 s), up to a maximum lag $\tau_{\rm fit}$, which was varied between 10 and 50 lags.

Finally, using the various (magnetic) scales, determined as outlined above, we calculate estimates for effective Reynolds numbers in three distinct ways. Specifically, we use $\lambda_C^{\rm fit}$ (or its timescale analog) as the outer scale and

(i) Equation (3) with d_i as the inner scale and $C_\epsilon^{-1/3} = 2$;
(ii) Equation (3) with $t_b = 1/(2\pi f_b)$ as the inner (time)scale and $C_\epsilon^{-1/3} = 2$;
(iii) Equation (5) with $\gamma/C_\epsilon = 27$.

4. Results

Our analysis uses data from the period 2004 June to December 2022 when Wind was always situated in the solar wind at L1. In about 6% of the intervals the slope of the kinetic range, q_k, was unusually shallow (meaning $|q_k| < 1.7$) and therefore the final (corrected) estimate of the Taylor scale came out to be negative. These outlier intervals were removed from the following analysis but will be investigated in future work.

4.1. Correlation Scale

Table 1 gives summary statistics of each of the three estimates of the correlation length of the magnetic field, λ_C, and Figure 5 shows their marginal and joint distributions. Given the wide distribution of values, all values are in line with those previously reported in the literature at 1 au, i.e., approximately 10^6 km (see Table 2). Noting the logarithmic scaling of the axes in this figure, we qualitatively find that the probability distribution function of each estimator is log-normal. This is consistent with the results of Ruiz et al. (2014) as well as the distribution of many other solar wind quantities such as proton temperature, plasma beta, and Alfvén speed (e.g., Hundhausen et al. 1970; Burlaga & Lazarus 2000; Mullan & Smith 2006; Veselovsky et al. 2010). In particular, the correlation scales are positively skewed, with means larger than the corresponding medians. Looking at the joint distributions, we see that the exponential fit and $1/e$ methods agree very well

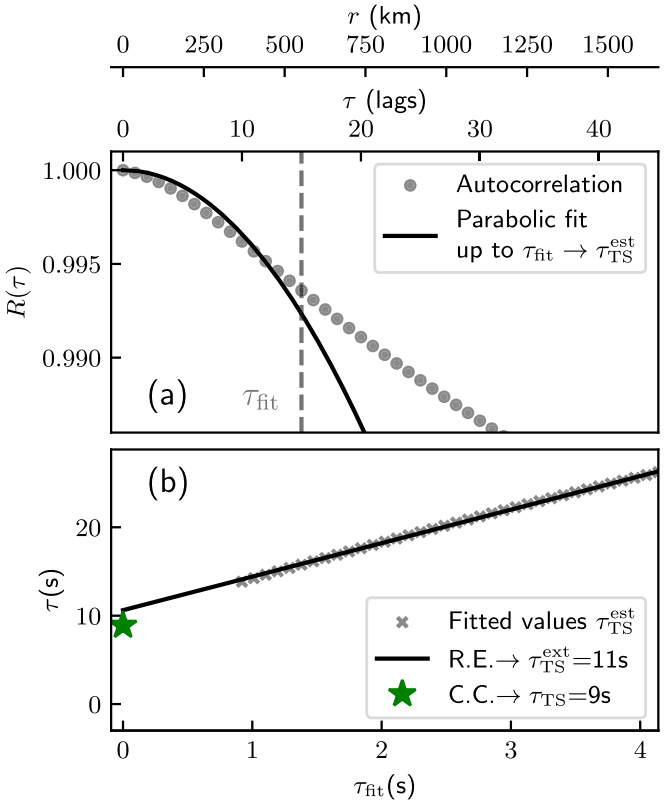

Figure 4. An example of the process of refining the estimate of the Taylor scale $\tau_{\rm TS}$, using an interval comprising the second half of 2016 January 2. The three horizontal scales show the separations in units of lag, time, and (Taylor frozen-flow equivalent) distance. (a) First, a parabola is fit to the autocorrelation from the origin up to various values of $\tau_{\rm fit}$. In this example the fit is for lags less than $\tau_{\rm fit} = 15$. The x-intercept of each parabola (which is off-scale for this plot) produces an initial estimate $\tau_{\rm TS}^{\rm est}$. (b) Next, each of these estimates is plotted against $\tau_{\rm fit}$. A straight line is fit to these points and extrapolated back to $\tau = 0$, returning the Richardson extrapolation (R.E.) estimate, $\tau_{\rm TS}^{\rm ext}$. Finally, the Chuychai correction (C.C.) is applied using the slope in the kinetic range ($q_k = -3.03$ in this case) in Equation (9). This yields our final estimate, $\tau_{\rm TS}$; we obtain a value of 9 s, or approximately 4000 km, for this particular interval.

Table 1
Statistical Summary of Estimates of the Magnetic Field Correlation Length λ_C by Different Methods

Method	Mean (km)	Median (km)	SE (km)
Exponential fit	899,000	769,000	5000
$1/e$	942,000	797,000	5000
Integral	880,000	808,000	4000

Note. The standard error (SE) gives the expected variation of the mean between samples of this size.

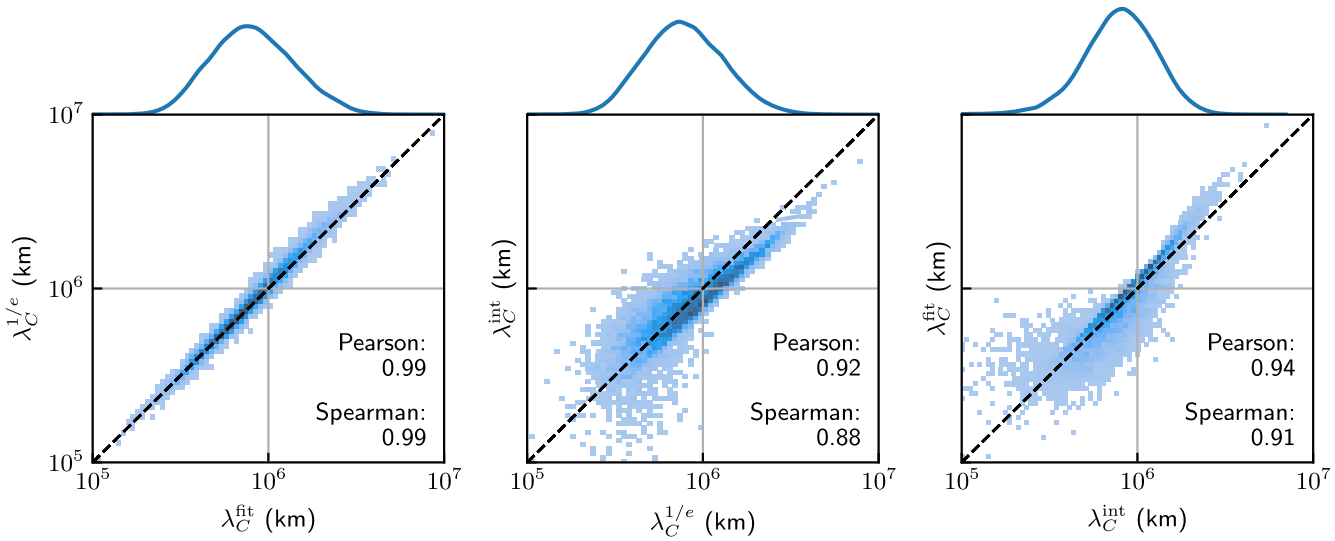

Figure 5. Joint (2D) histograms of the three λ_C estimates with Pearson (linear) correlation and Spearman (rank) correlation values and a dashed line of equality. Marginal (1D) histograms of the x-variable are shown above each plot. The x- and y-axis limits have been set so as to include the bulk of the data but exclude outliers. $\lambda_C^{\rm fit}$: exponential fit method, $\lambda_C^{1/e}$: $1/e$ method, $\lambda_C^{\rm int}$: integral method.

Table 2
Average Estimates of λ_C, λ_T, and an Effective Reynolds Number in the Solar Wind at 1 au, with the Last Calculated Using Equation (5)

Authors (Year)	Spacecraft	λ_C (10^6 km)	λ_T (km)	Re_{λ_T}	
Matthaeus et al. (2005)	ACE–Wind–Cluster	1.2	2478 ± 702	230,000	(×27)
Weygand et al. (2007)	Cluster	1.2 (from above)	2400 ± 100	260,000	(×27)
Weygand et al. (2009)	ACE–Wind–Cluster + 6 others	2.92	1000 ± 200	12,600,000	(×27)
Weygand et al. (2011)	ACE–Wind–Cluster + 8 others	1–2.8	1200–3500	4,000,000	(×27)
Zhou et al. (2020)	ACE–Wind–Cluster	1.14	2459	300,000[a]	(×27)
Bandyopadhyay et al. (2020)	MMS	0.32	6933	2000[b]	(×27)
This work	**Wind**	**0.899**	**3220**	**3,406,000**	

Notes. Shown are the values determined in this work (given in bold) and in some previous studies. Note that for direct comparison with this work, the Re_{λ_T} values from these earlier studies should be multiplied by the previously neglected prefactor of $\gamma/C_\epsilon = 27$, as indicated by the "(×27)" in the final column. This factor is already included in our estimates. When calculating λ_T all studies listed employed $\gamma = 3$, sometimes without explicitly stating so. All studies used at least one exponential fit to compute λ_C. All except Matthaeus et al. (2005) and Bandyopadhyay et al. (2020) used Richardson extrapolation to compute λ_T; none, other than this work, used the Chuychai correction. Values are expressed as ranges when the study grouped scales by other variables such as magnetic field orientation.
[a] This mean value was reported in a follow-up article (Zhou & He 2021).
[b] Re was not calculated explicitly in this article.

with each other, with very high values of 0.99 for both the Pearson and Spearman correlations, and most of the points lying close to the equality line. (The Spearman correlation uses ranks to measure the monotonicity of the relationship between two variables, rather than measure their linear association.) This agreement is not surprising given the large-scale statistical homogeneity of the solar wind. The autocorrelation functions typically show approximately exponential fall-off (see, e.g., Figure 3), with deviations from $\lambda_C^{1/e} \approx \lambda_C^{\rm fit}$ only occurring for intervals that do not show steady turbulence (Ruiz et al. 2014).

In contrast, the integral scale $\lambda_C^{\rm int}$ shows a moderate degree of scatter against either of the other two estimates, with correlations of between 0.88 and 0.94. The greatest degree of scatter is present for values of $\lambda_C^{\rm int}$ less than about 10^6 km. This disagreement is likely due to occasional numerical issues with calculating the integral of the autocorrelation. Ideally, the integral is computed out to infinity as R asymptotically decays to 0. However, the finite size of the intervals and the slight departures from "textbook-like" homogeneity and isotropy in some intervals could introduce discrepancies between this and the exponential estimates. Nonetheless, we conclude that, to a reasonable approximation, all three methods give equivalent estimates for λ_C.

4.2. Taylor Scale

Figure 6 shows marginal distributions of both the uncorrected and corrected versions of λ_T for the magnetic field. Both have quasi-Gaussian distributions, with a few large outliers. The distribution of λ_T computed after applying the Chuychai correction factor is shifted to the left because the (multiplicative) correction factor is almost always less than 1, except for the 1% of intervals with particularly steep slopes in the kinetic range ($q_k < -3.7$). The mean q_k is -2.64, resulting in an average correction factor of $-2.61/2.64 + 1.7 = 0.71$, following Equation (9). We therefore end up with a mean of λ_T that is about two thirds that of $\lambda_T^{\rm ext}$. We find that this final mean of 3225 km is in good agreement with the literature (see Table 2). Prior estimates of λ_T in the solar wind at 1 au vary between ∼1000 km and ∼7000 km, values that lie within the distributions of λ_T (extrapolated or Chuychai-corrected) shown in Figure 6.

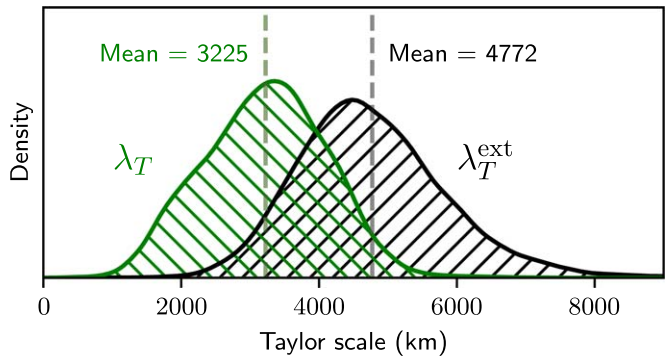

Figure 6. Distributions of the uncorrected ($\lambda_{\rm T}^{\rm ext}$) and corrected ($\lambda_{\rm T}$) versions of the Taylor scale. Dashed vertical lines indicate mean values for each distribution. The x-axis limits have been set so as to include the bulk of the data but exclude outliers.

4.3. Reynolds Number

Having obtained estimates for the correlation length and Taylor scale of the magnetic field fluctuations (and also for d_i and t_b), we may use the procedures detailed at the end of Section 3 to calculate three distinct effective Reynolds numbers. Figure 7 shows the marginal and joint distributions of these different estimates, as well as regression line fits. After applying a logarithmic transformation each distribution appears approximately Gaussian, suggesting a log-normal distribution. Comparing these marginal distributions and the summary statistics given in Table 3, we can see that the three estimates span multiple orders of magnitude, with, very roughly, $Re_{\lambda_{\rm T}} \approx 10\, Re_{d_i} \approx 30\, Re_{t_b}$ for the mean values.

The joint distributions show considerably more scatter than those of the λ_C estimates. The strongest linear association between any two estimates is that between Re_{d_i} and Re_{t_b} (Pearson correlation = 0.72). This is shown by the majority of points lying in a relatively thin linear band close to the equality line. We can also see that the Re_{t_b} estimates tend to be smaller than Re_{d_i}. This is an indication that the break scale is typically larger than d_i by a factor of 2–3 in the solar wind (Leamon et al. 1998). A dependence of the break scale on plasma β is also well known (Chen et al. 2014; Franci et al. 2016). The statistical details of any such potential correlations will be explored in a follow-up study.

$Re_{\lambda_{\rm T}}$ shows a much weaker linear association with the other two methods of only 0.38 (with Re_{d_i}) and 0.43 (with Re_{t_b}). In addition to having the lowest Pearson correlation, $Re_{\lambda_{\rm T}}$ and Re_{t_b} also have the lowest Spearman correlation, showing that even after accounting for outliers, which have less influence on this latter metric, it still remains a rather weakly positive association. On the other hand, outliers do have a clear influence on the linear association of $Re_{\lambda_{\rm T}}$ versus Re_{d_i}, shown by the substantial increase in the Spearman correlation (0.74) over the Pearson correlation (0.38).

Despite these only moderately strong associations between the estimates, it is important to note the density of the points. All these distributions show significant scatter of a small population in which the estimates differ by up to an order of magnitude. Notably, the joint distributions of Re_{t_b} have a roughly triangular subpopulation of points that shows little to no relationship with the other estimates. This is seen in the upper left of the plot of $Re_{\lambda_{\rm T}}$ versus Re_{t_b}, and the lower right of Re_{t_b} versus Re_{d_i}. This population (identified as $Re_{\lambda_{\rm T}}/Re_{t_b}>50$) represents about 27% of all observations and is shown as the gray points in Figure 7. After removing this population, all correlations increase to at least 0.68. The potential reasons for significantly larger t_b and hence a smaller Re_{t_b} could include errors in automated fitting and extreme intervals with atypical power spectra. As with the other outliers, a detailed investigation of these is deferred to a follow-up study. In cases where the power spectrum is well behaved, with typical slopes in the inertial and kinetic ranges (q_i and q_k) and a well-defined break point, it might be safe to estimate Re_{tb} and multiply it by 30 to estimate $Re_{\lambda_{\rm T}}$.

As well as the agreement between methods, it is also of interest how our estimates of Re match up with those previously reported. In particular, given the prevalence of the Taylor scale method, we compare values of Re_{λ_T} in Table 2. The values for Re in this table vary by a factor of ≈6000, from 54,000 to 340,000,000 after multiplying by the prefactor. The mean value of $Re_{\lambda_{\rm T}}$=3,406,000 from the present study is of the same order of magnitude as the results from three of the previous works. The much larger values given in Weygand et al. (2009, 2011) were mainly attributed to the smaller values obtained for $\lambda_{\rm T}$. Conversely, Bandyopadhyay et al. (2020) noted that their value of $\lambda_{\rm T}$ calculated from a single 5 hr interval of MMS data was about three times larger than previous estimates, while their estimation of λ_C was smaller than other estimates. Hence they computed a much smaller value of Re. Three reasons were suggested for this: (1) interval length, separation, and mixing effects, (2) intrinsic variability in the solar wind, and (3) differences in the geometric formations of the Cluster (to which they were comparing their results) and MMS spacecraft. Our work herein emphasizes that point (2) is indeed pertinent. In particular, our results show the considerable intrinsic variability of the properties of the solar wind (particularly λ_C and $\lambda_{\rm T}$), giving rise to large variability in the values of effective Re. On the plus side, this sampling variability suggests that the results of all the cited studies may in fact be consistent with each other, as they lie within the distribution of values found in our study.

5. Conclusion

We present a thorough investigation and review of calculating estimates of (effective) Reynolds numbers for the solar wind at 1 au, using 18 years of data from NASA's Wind spacecraft. As this data set lacks high-time-cadence velocity measurements, we employ magnetic field data to estimate λ_C and $\lambda_{\rm T}$ for the magnetic field. These are assumed to be comparable to their velocity field equivalents, in line with previously published results. More precisely, in using the magnetic length scales in Equation (5) we are assuming that $\lambda_C^b/\lambda_{\rm T}^b \approx \lambda_C^v/\lambda_{\rm T}^v$.

We first compare three different ways of calculating the correlation scale and find good agreement between all methods, albeit with a greater scatter for the integral method. The mean values obtained for λ_C, between 880,000 and 942,000 km, are consistent with previously reported values of about 10^6 km.

We then apply the correction factor developed by Chuychai et al. (2014) to our estimates of the Taylor scale in order to reduce any remaining bias after using the Richardson extrapolation technique. This correction factor typically reduces the estimate of the Taylor scale, significantly shifting the distribution to smaller values. In particular, the mean reduces to 3225 km, roughly 2/3 of the uncorrected mean value

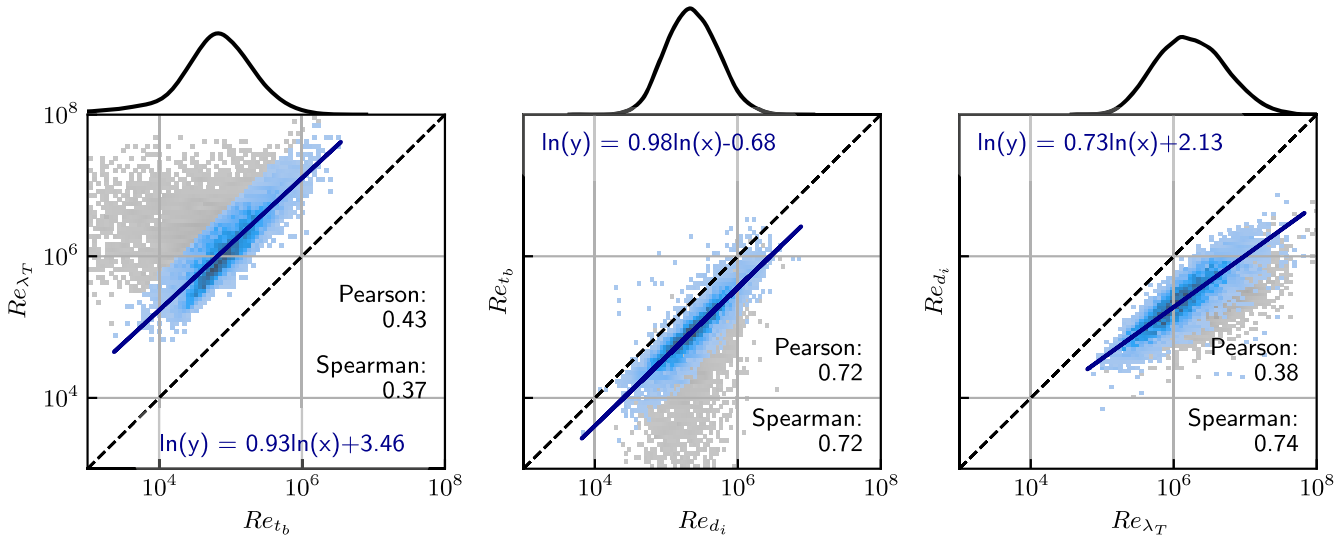

Figure 7. Joint (2D) histograms of the three *Re* estimates with Pearson correlation and Spearman (rank) correlation values, log-space regression line fits, and a dashed line of equality; and (above top axis) marginal (1D) histograms of the *x*-variable in each plot. The *x*- and *y*-axis limits have been set so as to include the bulk of the data but exclude particularly extreme outliers beyond these limits. Remaining outliers are shaded gray. Correlation coefficients and marginal histograms are for all data values, whereas regression lines are fitted to only the majority subsets of the data shown in blue (see text).

Table 3
Statistical Summary of the Estimates of Effective *Re* Obtained by the Different Methods

Re	Mean	Median	SE
Re_{t_b}	116,000	64,000	2000
Re_{d_i}	330,000	226,000	3000
Re_{λ_T}	3,406,000	1,686,000	68,000

Note. SE = standard error of the mean.

of 4772 km. Both values are consistent with previous estimates, given the wide spread of the distribution.

Finally, we compute effective Reynolds numbers using three distinct methods. It should be noted that we include proportionality factors in our calculations. In particular, we highlight that the factor in Re_{λ_T} of $C_\epsilon \approx 27$ was not included in many previously published estimates (see Table 2 and Equation (5)).

While very strong correlations were observed for the three different methods of estimating λ_C, the correlations between the associated estimates of the effective Reynolds number were only moderate to strong, with a considerable amount of scatter. The mean values determined by these methods ranged from 116,000 for Re_{t_b} to 3,406,000 for Re_{λ_T}. Putting these into perspective, previously reported values of *Re* at 1 au exhibit substantial variability, ranging from approximately 10^6 to 10^8. Most of our estimates of *Re* comfortably fit within this distribution, though an outlier population of small values of Re_{t_b} warrants future investigation.

Ultimately, we conclude that more theoretical work is needed to better understand which definition of an effective Reynolds number of the solar wind is most appropriate. The key task is to identify scales that have a physical meaning. For the t_b or d_i approximations of the inner scale, the implication is that ion-scale physics plays the most significant role in energy dissipation and terminates the inertial range. This, however, discounts the role of a sub-ion-scale cascade and its implications for electron physics (Matthaeus et al. 2008; Alexandrova et al. 2009; Sahraoui et al. 2009; Schekochihin et al. 2009; Boldyrev et al. 2013). Moreover, these estimates are insensitive to the variability of the power input at large scales and hence the cascade rate. On the other hand, the λ_T-based estimate of *Re* indirectly folds in the cascade rate through its dependence (empirically in the solar wind but directly in hydrodynamics) (Pope 2000; Matthaeus et al. 2008). This makes Re_{λ_T} a more physically motivated estimate among the three considered.

Moreover, having obtained statistical relationships between different estimates, these can be leveraged in situations where only one estimate is calculable. The decision on which estimator to use rests on the assumptions one elects to make and on the resolution of the available data. These considerations are summarized below.

1. Re_{t_b} requires calculation of the spectral break scale. This process is subject to varying methods and numerical challenges, including spectra that do not always show clear breaks. In our work, we calculated t_b as the intersection of (the extrapolation of) two power-law fits to magnetic field spectra, which requires decisions on what intervals to choose for the inertial and dissipation ranges.
2. Alternatively, one can simply use the ion inertial length d_i to approximate the break scale and calculate Re_{d_i} (Parashar et al. 2019; Cuesta et al. 2022b). This requires only the ion density (and correlation length). However, it appears that changing solar wind conditions affect which scale is best associated with the spectral break. Specifically, d_i is the best approximation at low plasma β values, the ion gyroradius ρ_i is best at high β values (Chen et al. 2014), and for typical solar wind values of $\beta \approx 1$, the ion cyclotron resonance scale is the best (Woodham et al. 2018). Under conditions where one might not have high-time-cadence measurements of the desired variables, it is likely that one could still easily obtain reasonable estimates for both d_i and the outer scale (e.g., λ_C) and employ these to estimate an effective Reynolds number.

3. Using the Taylor scale-based Reynolds number, Re_{λ_T}, is a more robust formulation for estimating Re than the two listed above because of its empirical dependence on the cascade rate (Matthaeus et al. 2008). This benefit is shown by the prevalence of this formulation in the literature (Matthaeus et al. 2005; Weygand et al. 2007, 2009, 2011; Zhou et al. 2020; Phillips et al. 2022). We show here that the use of a correction factor (Chuychai et al. 2014) makes a significant difference in the estimates of λ_T and hence Re_{λ_T}. However, as discussed above, the λ_T definition of Re has a proportionality factor that is, in part, determined by a phenomenological or empirical fitting for the (kinetic energy) dissipation rate. Calculating λ_T also requires high-resolution data, which are not always available; for example, Voyager observations of the outer heliosphere are so restricted (Parashar et al. 2019). Furthermore, while this does not affect the validity of this formulation, we note that weak cascade rates have been shown to result in λ_T being smaller than the break scale, inverting the hydrodynamic ordering (Matthaeus et al. 2008). This is believed to be due to greater relevance of electron dissipation (relative to proton) in these circumstances of a weak cascade (Matthaeus et al. 2016).

A limitation of this work is that it relies on the Taylor hypothesis to convert from single-spacecraft time separations to length separations. This assumes that the bulk flow is sufficiently fast that local variations in time can be effectively ignored (see Verma 2022, for solar wind context). The Taylor hypothesis relates to the well-studied "sweeping" hypothesis, whereby large-scale fluctuations sweep (i.e., advect) smaller-scale fluctuations (Kraichnan 1965; Tennekes 1975; Zhou 2021). Although invoking Taylor's hypothesis at kinetic scales might introduce substantial inaccuracies, it has nonetheless been shown, numerically and from observations, to be a reasonably good approximation up to second-order statistics (Perri et al. 2017; Chhiber et al. 2018; Roberts et al. 2022). This is also true under a model that incorporates sweeping phenomenology (Bourouaine & Perez 2019; Perez et al. 2021). Furthermore, for the present analysis, we note that this assumption does not affect the results for Re_{λ_T}, because both of the scales involved are in fact left as timescales for this calculation. Another aspect that we did not address in this study is the issue of anisotropy in λ_C and λ_T (e.g., Weygand et al. 2009, 2011; Cuesta et al. 2022a; Roy et al. 2022). We reiterate that no data filtering was conducted, except to remove intervals with significant missing data, limit the time period for analysis to 2004 June onward, and remove outliers where $|q_k| < 1.7$.

Finally, we envisage that the full 28 yr data set and the accompanying code that we have provided as a data product will be useful to the scientific community for future large-scale statistical analysis and data mining, for Wind and other missions. Future work will start investigating correlations, dimensionality reduction, and machine learning models.

Acknowledgments

We are grateful to the Wind MFI and 3DP instrument teams for the data and NASA GSFC's Space Physics Data Facility for providing access to it.[3] We acknowledge the World Data Center SILSO at the Royal Observatory of Belgium in Brussels for providing the sunspot data.[4] We also thank Bill Matthaeus for providing feedback on the manuscript.

Author Contributions

1. T.N.P.: conceptualized and supervised the project and edited the draft manuscript.
2. D.W.: refined and extended the pipeline, created the final data set, and wrote the draft manuscript.
3. S.O.: identified and calculated the prefactors in the Reynolds number equations.
4. K.D.L.: conducted preliminary analysis with guidance from T.N.P. and M.F.
5. All authors discussed results and implications and helped edit the final manuscript.

Appendix A
Determination of the C_ϵ Prefactor for MHD

A standard phenomenological estimate for the kinetic energy dissipation rate (ϵ^v) in Navier–Stokes turbulence is

$$\epsilon_{\rm phenom} = A\frac{u_1^3}{\ell_f^v} = C_\epsilon \frac{U^3}{\lambda_C} \tag{A1}$$

(e.g., Batchelor 1970; Tennekes & Lumley 1972; Pope 2000). Here, $\langle \boldsymbol{v}\cdot\boldsymbol{v}\rangle = U^2$ and u_1 is the rms velocity for one component of $\boldsymbol{v}$. Also ℓ_f^v is the correlation length associated with the longitudinal correlation function (Batchelor 1970), whereas λ_C is that for the traced correlation function $R^v(r) = \langle \boldsymbol{v}(\boldsymbol{x})\cdot\boldsymbol{v}(\boldsymbol{x}+\boldsymbol{r})\rangle$, equivalent to our λ_C definition in the main text. The dimensionless coefficients A and C_ϵ are treated as constants that may be determined using experiments and/or simulations (Sreenivasan 1998; Pearson et al. 2004). For isotropic 3D turbulence, the relations $U^2 = 3u_1^2$, $\lambda_C = 2\ell_f^v/3$, and $C_\epsilon = 2A/(9\sqrt{3})$ hold. As the middle "component-based" version is founded on the assumption of isotropy, in this work we instead employ the rightmost "trace-based" variant, which does not assume isotropy; this is given as Equation (2) above. (When the turbulence is isotropic and two-dimensional, one obtains $C_\epsilon = A(4\sqrt{2})$, which is ≈40% larger than the 3D isotropic value.)

In the literature a variety of notations are in use for what we have called A and C_ϵ, and indeed some works use C_ϵ for the A in Equation (A1) (e.g., Pearson et al. 2004); clearly this should not be confused with the C_ϵ we employ herein. For clarity, and in line with the notation of Batchelor (1970, Equation (6.1.1)), we always use A to denote a component-based fitting value.

We wish to determine a value for C_ϵ that is applicable in MHD. This requires taking into account the dissipation of magnetic as well as kinetic energy. With superscripts v and b denoting velocity and magnetic quantities, respectively, we may write the total energy decay rate as $\epsilon^{\rm MHD} = \epsilon^v + \epsilon^b$.

Using an Elsässer variable ($\boldsymbol{z}_\pm = \boldsymbol{v} \pm \boldsymbol{b}$) and von Kármán–Howarth equation analysis for incompressible MHD, Linkmann et al. (2015, 2017) developed a theory for $A^{\rm MHD}$ (denoted $C_{\epsilon,\infty}$ therein). For simplicity here we restrict attention to situations with low cross-helicity, i.e., $\langle \boldsymbol{v}\cdot\boldsymbol{b}\rangle \approx 0$. Consequently, $\langle|\boldsymbol{z}_+|^2\rangle \approx \langle|\boldsymbol{z}_-|^2\rangle = Z^2 = 3W^2$, and the two longitudinal

[3] https://spdf.gsfc.nasa.gov/

[4] http://www.sidc.be/silso/

Elsässer correlation lengths, $\ell_f^{\pm}$, are approximately equal. Assuming further that the longitudinal correlation lengths for $\boldsymbol{v}$ and $\boldsymbol{b}$ are also approximately equal, the (low cross-helicity) result of Linkmann et al. is equivalent to

$$\epsilon_{\rm phenom}^{\rm MHD} = A\frac{W^3}{\ell_f^+} = \frac{2A}{9\sqrt{3}}\frac{Z^3}{\lambda_C^v}, \tag{A2}$$

where $A \equiv A^{\rm MHD}$ and we have made use of the isotropic relation $\ell_f^v = \frac{3}{2}\lambda_C^v$. Equation (A2) applies to the total (viscous plus resistive) dissipation and is the MHD analog of Equation (2) above. Although, formally, it only applies for cases of low cross-helicity, it is likely to be approximately valid under somewhat more general circumstances (Linkmann et al. 2017; Bandyopadhyay et al. 2018).

Next, we make use of the Alfvén ratio, $r_{\rm A} = U^2/\langle \boldsymbol{b}^2\rangle$, to write $\epsilon^{\rm MHD}$ in terms of ϵ^v. In terms of U and $r_{\rm A}$, the zero-cross-helicity form for Z^2 is

$$Z^2 \;=\; U^2 + \langle \boldsymbol{b}^2\rangle = U^2\left(1+\frac{1}{r_{\rm A}}\right) = U^2F(r_{\rm A}), \tag{A3}$$

which defines $F(r_{\rm A})$.

Recall also that $\epsilon^{\rm MHD} = \nu\langle\boldsymbol{\omega}^2\rangle + \mu\langle \boldsymbol{j}^2\rangle$, with ν the kinematic viscosity, μ the magnetic resistivity, $\boldsymbol{\omega} = \nabla\times\boldsymbol{v}$ the vorticity, and $\boldsymbol{j} = \nabla\times\boldsymbol{b}$ the electric current density. Assuming a Prandtl number of order unity ($\nu \approx \mu$) and that $\langle \boldsymbol{j}^2\rangle/\langle\boldsymbol{\omega}^2\rangle \approx 1/r_{\rm A}$, as is commonly seen in MHD simulations, $\epsilon^{\rm MHD}$ can be re-expressed without explicit reference to the dissipation coefficients:

$$\epsilon^{\rm MHD} \approx \epsilon^v F(r_{\rm A}). \tag{A4}$$

Finally, using Equations (A2) and (A4), we can write a (small cross-helicity) approximation for the kinetic energy dissipation rate in MHD:

$$\epsilon^v \approx \left(\frac{2A}{9\sqrt{3}}\sqrt{F}\right)\frac{U^3}{\lambda_C}. \tag{A5}$$

The bracketed factor might be called $C_\epsilon^{{\rm MHD},v}$ and can be identified with C_ϵ in our Equation (2). Observationally, for the solar wind, $r_{\rm A}\approx 1/2$, yielding $F\approx 3$ (e.g., Perri & Balogh 2010). Results from MHD simulations (Linkmann et al. 2017; Bandyopadhyay et al. 2018)[5] indicate that $A\approx 0.5$ for situations with zero or moderate mean magnetic field and low or moderate cross-helicity, as is relevant to the solar wind. Using these values we obtain $C_\epsilon^{{\rm MHD},v}\approx 0.11$, which is about twice the hydrodynamics estimate of $C_\epsilon^{\rm hydro}\approx 0.064$ (via $A\approx 0.5$); see Sreenivasan (1998) and Pearson et al. (2004). This gives us values for the prefactor of Equation (5) of $\frac{\gamma}{C_\epsilon} = \frac{3}{0.11}\approx 27$, and of Equation (3) of $C_\epsilon^{1/3}\approx 2$.

The results obtained in this appendix are most relevant for systems governed by the incompressible collisional 3D MHD equations. Thus, application of these results to the nearly collisionless solar wind needs to be undertaken with caution.

[5] In both these works A is denoted as $C_{\epsilon,\infty}$ and here we employ double their numerical value for A because of a definitional difference between their $L_\pm$ and our $\ell_f^\pm$.

Appendix B
Data Product

Averages of each variable in our data set are given in Table 4. The data set (in CSV form), along with metadata describing the variables and the code used to extract and process the data, is available on GitHub[6] under a 2-Clause BSD

Table 4
List of the Key Variables in Our Wind Data Product, Comprising Statistics for Every 12 hr from 1995 to 2022

Symbol	Name	Mean Value	Unit
SN	Sunspot number	56.3	⋯
$M_{\rm A}$	Alfvén Mach number	7.36	⋯
M_s	Sonic Mach number	15.31	⋯
$\beta_{\rm e}$	Electron plasma beta	0.82	⋯
$\beta_{\rm p}$	Proton plasma beta	0.53	⋯
σ_c	Cross-helicity	0.01	⋯
σ_R	Residual energy	−0.44	⋯
$R_{\rm A}$	Alfvén ratio	0.46	⋯
cos(A)	Alignment cosine	0.01	⋯
q_i	Slope in the inertial range	−1.68	⋯
q_k	Slope in the kinetic range	−2.64	⋯
$Re_{\lambda_{\rm T}}$	Reynolds number ($\lambda_{\rm T}$)	3,406,000	⋯
Re_{d_i}	Reynolds number (d_i)	330,000	⋯
Re_{t_b}	Reynolds number (t_b)	116,000	⋯
$\delta b/B_0$	Normalized magnetic field fluctuations	0.71	...
f_b	Spectral break frequency	0.25	Hz
t_b	Spectral break timescale	14.3	s
B_0	Magnetic field magnitude (rms)	5.49	nT
δb	Magnetic field fluctuations (rms)	3.83	nT
$n_{\rm e}$	Electron density	4.18	$\rm cm^{-3}$
n_α	Alpha density	0.14	$\rm cm^{-3}$
$T_{\rm e}$	Electron temperature	12.9	eV
$T_{\rm p}$	Proton temperature	11.0	eV
T_α	Alpha temperature	63.8	eV
$\rho_{\rm e}$	Electron gyroradius	1.78	km
$\rho_{\rm p}$	Proton gyroradius	63.9	km
$d_{\rm e}$	Electron inertial length	3.12	km
d_i	Proton inertial length	134	km
l_d	Debye length	0.02	km
$\lambda_C^{\rm fit}$	Correlation length scale (exp. fit)	899,000	km
$\lambda_C^{\rm exp}$	Correlation length scale ($1/e$)	942,000	km
$\lambda_C^{\rm int}$	Correlation length scale (integral)	880,000	km
$\lambda_{\rm T}^{\rm ext}$	Taylor length scale (raw)	4770	km
$\lambda_{\rm T}$	Taylor length scale (corrected)	3220	km
V_0	Velocity magnitude (rms)	439	$\rm km\,s^{-1}$
V_r	Radial velocity	438	$\rm km\,s^{-1}$
δv	Velocity fluctuations (rms)	26.2	$\rm km\,s^{-1}$
$v_{\rm A}$	Alfvén speed	65.5	$\rm km\,s^{-1}$
$v_{T_{\rm e}}$	Electron thermal velocity	1490	$\rm km\,s^{-1}$
$v_{T_{\rm p}}$	Proton thermal velocity	30.5	$\rm km\,s^{-1}$
$\delta b_{\rm A}$	Magnetic field fluctuations (Alfvén units, rms)	42.4	$\rm km\,s^{-1}$
z^+	Positive Elsässer variable (rms)	48.9	$\rm km\,s^{-1}$
z^-	Negative Elsässer variable (rms)	48.4	$\rm km\,s^{-1}$

Note. The mean values are for the cleaned 18 yr data set at L1 used in this study. While not shown here, we also provide a few additional variables such as the timescale versions of the length scales, the uncertainty of the Taylor scale, and the amount of missing data for each raw interval. The complete metadata, including the equations used to derive secondary variables such as gyroradii and cross-helicity, can be found in the GitHub README.

[6] `reynolds_scales_project` codebase: https://github.com/daniel-wrench/reynolds_scales_project.

License and is archived in Zenodo (Wrench 2023). The code has been designed so as to make it relatively simple to apply to data from other missions available in CDAWeb. That is, it should be straightforward to adapt for projects interested in calculating these variables for different heliophysics and space weather environments.

ORCID iDs

Daniel Wrench https://orcid.org/0000-0002-7463-3818
Tulasi N. Parashar https://orcid.org/0000-0003-0602-8381
Sean Oughton https://orcid.org/0000-0002-2814-7288
Marcus Frean https://orcid.org/0000-0001-5840-8760

References

Alexandrova, O., Saur, J., Lacombe, C., et al. 2009, PhRvL, 103, 165003
Balbus, S. A., & Hawley, J. F. 1998, RvMP, 70, 1
Bandyopadhyay, R., Matthaeus, W. H., Chasapis, A., et al. 2020, ApJ, 899, 63
Bandyopadhyay, R., Oughton, S., Wan, M., et al. 2018, PhRvX, 8, 041052
Bandyopadhyay, R., Yang, Y., Matthaeus, W. H., et al. 2023, PhPl, 30, 080702
Batchelor, G. K. 1970, The Theory of Homogeneous Turbulence (Cambridge: Cambridge Univ. Press)
Boldyrev, S., Horaites, K., Xia, Q., & Perez, J. C. 2013, ApJ, 777, 41
Bourouaine, S., & Perez, J. C. 2019, ApJL, 879, L16
Bruno, R., & Carbone, V. 2013, LRSP, 10, 2
Burlaga, L. F., & Lazarus, A. J. 2000, JGR, 105, 2357
Cartagena-Sanchez, C. A., Carlson, J. M., & Schaffner, D. A. 2022, PhPl, 29, 032305
Chapman, S., & Cowling, T. G. 1990, The Mathematical Theory of Non-uniform Gases: An Account of the Kinetic Theory of Viscosity, Thermal Conduction and Diffusion in Gases (Cambridge: Cambridge Univ. Press)
Chen, C. H. K., Leung, L., Boldyrev, S., Maruca, B. A., & Bale, S. D. 2014, GeoRL, 41, 8081
Cheng, L., & Wang, Y. 2022, ApJ, 941, 37
Chhiber, R., Chasapis, A., Bandyopadhyay, R., et al. 2018, JGRA, 123, 9941
Chuychai, P., Weygand, J. M., Matthaeus, W. H., et al. 2014, JGRA, 119, 4256
Cuesta, M. E., Chhiber, R., Roy, S., et al. 2022a, ApJL, 932, L11
Cuesta, M. E., Parashar, T. N., Chhiber, R., & Matthaeus, W. H. 2022b, ApJS, 259, 23
Czaykowska, A., Bauer, T. M., Treumann, R. A., & Baumjohann, W. 2001, AnGeo, 19, 275
Franci, L., Landi, S., Matteini, L., Verdini, A., & Hellinger, P. 2016, ApJ, 833, 91
Hadid, L., Sahraoui, F., Kiyani, K. H., et al. 2015, ApJL, 813, L29
Hinze, J. 1975, in Turbulence, McGraw-Hill Classic Textbook Reissue, ed. B. J. Clark (2nd ed.; New York: McGraw-Hill)
Huang, K. 2008, Statistical Mechanics (New York: Wiley)
Huang, S., Hadid, L., Sahraoui, F., Yuan, Z., & Deng, X. 2017, ApJL, 836, L10
Hundhausen, A., Bame, S., Asbridge, J., & Sydoriak, S. 1970, JGR, 75, 4643
Isaacs, J. J., Tessein, J. A., & Matthaeus, W. H. 2015, JGRA, 120, 868
Kolmogorov, A. N. 1941, DoSSR, 30, 301
Kraichnan, R. H. 1965, PhFl, 8, 1385
Leamon, R. J., Smith, C. W., Ness, N. F., Matthaeus, W. H., & Wong, H. K. 1998, JGR, 103, 4775
Lepping, R. P., Slavin, J. A., Ness, N. E., et al. 1995, SSRv, 71, 207
Linkmann, M., Berera, A., & Goldstraw, E. E. 2017, PhRvE, 95, 013102
Linkmann, M. F., Berera, A., McComb, W. D., & McKay, M. E. 2015, PhRvL, 114, 235001
Lotz, S., Nel, A. E., Wicks, R. T., et al. 2023, ApJ, 942, 93
Marsch, E. 2006, LRSP, 3, 1
Matthaeus, W. H., Dasso, S., Weygand, J. M., et al. 2005, PhRvL, 95, 231101
Matthaeus, W. H., Parashar, T. N., & Wan, M. 2016, ApJL, 827, L7
Matthaeus, W. H., Wan, M., Servidio, S., et al. 2015, RSPTA, 373, 20140154
Matthaeus, W. H., Weygand, J. M., Chuychai, P., et al. 2008, ApJ, 678, 141
Mohapatra, R., Federrath, C., & Sharma, P. 2020, MNRAS, 493, 5838
Mullan, D., & Smith, C. 2006, SoPh, 234, 325
Parashar, T. N., Cuesta, M., & Matthaeus, W. H. 2019, ApJL, 884, L57
Parashar, T. N., Matthaeus, W. H., Shay, M. A., & Wan, M. 2015, ApJ, 811, 112
Pearson, B. R., Yousef, T. A., Haugen, N. E. L., Brandenburg, A., & Krogstad, P. A. 2004, PhRvE, 70, 056301
Perez, J. C., Bourouaine, S., Chen, C. H. K., & Raouafi, N. E. 2021, A&A, 650, A22
Perri, S., & Balogh, A. 2010, GeoRL, 37, L17102
Perri, S., Servidio, S., Vaivads, A., & Valentini, F. 2017, ApJS, 231, 4
Phillips, C., Bandyopadhyay, R., & McComas, D. J. 2022, ApJ, 933, 33
Pope, S. B. 2000, Turbulent Flows (Cambridge: Cambridge Univ. Press)
Roberts, O. W., Alexandrova, O., Sorriso-Valvo, L., et al. 2022, JGRA, 127, e2021JA029483
Roy, S., Chhiber, R., Dasso, S., Ruiz, M. E., & Matthaeus, W. H. 2022, PhRvE, 105, 045204
Ruiz, M. E., Dasso, S., Matthaeus, W. H., & Weygand, J. M. 2014, SoPh, 289, 3917
Sahraoui, F., Goldstein, M., Robert, P., & Khotyaintsev, Y. V. 2009, PhRvL, 102, 231102
Schekochihin, A., Cowley, S., Dorland, W., et al. 2009, ApJS, 182, 310
Sreenivasan, K. R. 1998, PhFl, 10, 528
Taylor, G. I. 1935, RSPSA, 151, 421
Tennekes, H. 1975, JFM, 67, 561
Tennekes, H., & Lumley, J. L. 1972, A First Course in Turbulence (Cambridge, MA: MIT Press)
van Atta, C., & Antonia, R. 1980, PhFl, 23, 252
Verma, M. K. 1996, JGRA, 101, 27543
Verma, M. K. 2022, PhPl, 29, 082902
Veselovsky, I., Dmitriev, A., & Suvorova, A. 2010, CosRe, 48, 113
Wang, X., Tu, C., He, J., & Wang, L. 2018, JGRA, 123, 68
Weygand, J. M., Matthaeus, W. H., Dasso, S., et al. 2009, JGRA, 114, A07213
Weygand, J. M., Matthaeus, W. H., Dasso, S., & Kivelson, M. G. 2011, JGRA, 116, A08102
Weygand, J. M., Matthaeus, W. H., Dasso, S., Kivelson, M. G., & Walker, R. J. 2007, JGRA, 112, A10201
Wilson, L. B., III, Brosius, A. L., Gopalswamy, N., et al. 2021, RvGeo, 59, e2020RG000714
Woodham, L. D., Wicks, R. T., Verscharen, D., & Owen, C. J. 2018, ApJ, 856, 49
Wrench, D. 2023, reynolds_scales_project, v2.0, Zenodo, doi:10.5281/ZENODO.8352767
Yang, Y., Matthaeus, W. H., Oughton, S., et al. 2023, arXiv:2309.02663
Yang, Y., Matthaeus, W. H., Roy, S., et al. 2022, ApJ, 929, 142
Zhou, G., & He, H. Q. 2021, ApJL, 911, L2
Zhou, G., He, H. Q., & Wan, W. 2020, ApJL, 899, L32
Zhou, Y. 2007, PhPl, 14, 082701
Zhou, Y. 2017, PhR, 720, 1
Zhou, Y. 2021, PhR, 935, 1
Zhou, Y., Grinstein, F. F., Wachtor, A. J., & Haines, B. M. 2014, PhRvE, 89, 013303
Zhou, Y., & Thornber, B. 2016, ATJFE, 138, 070905
Zhuravleva, I., Churazov, E., Schekochihin, A., et al. 2019, NatAs, 3, 832